Journal of Applied Biology & Biotechnology Vol. 13(4), pp. 126-135, July-August, 2025
Available online at http://www.jabonline.in
DOI: 10.7324/JABB.2025.220729

Green synthesised *Catharanthus roseus*-mediated iron oxide nanoparticles demonstrates enhanced antibacterial, antioxidant, and anti-diabetic properties

Priya Josson Akkara*, Sonia Angeline Martin, Nathiya Thiagarajulu, Aanchal Bisht Bisht, Archana Mishal, Christina M. Mathew

Department of Life Sciences, Kristu Jayanti College, Bangalore, India.

ARTICLE INFO

Article history:
Received on: November 16, 2024
Accepted on: March 05, 2025
Available Online: May 25, 2025

Key words:
Catharanthus roseus-iron oxide nanoparticles, green synthesis, antibacterial, antioxidant, antidiabetic

ABSTRACT

The therapeutic possibility of *Catharanthus roseus* ethanolic extract of leaves (CELEs) was related with that of *C. roseus* mediated green synthesized iron oxide nanoparticles (CELFeNPs) for its antibacterial, antioxidant, as well as anti-diabetic activities. The bioactive components in CELE were assessed by gas chromatography-mass spectrometry to prepare Fe_2O_3 nanoparticles (CELFeNPs) utilizing the phytoreducing method of green synthesis. Fourier transform-infrared spectroscopy analysis was performed to analyze the capping of nanoparticles by phytochemicals, and the crystalline nature was validated by X-ray diffraction analysis. Comparative antioxidant activity was assayed by 2,2-Diphenyl-1-picrylhydrazyl and ferric reducing antioxidant power assay, antidiabetic effect was evaluated by alpha-amylase inhibitory activity, and antibacterial activity was assessed. CELFeNPs showed enhanced antioxidant activity than CELE. The antibacterial efficacy of CELFeNPs improved with increased nanoparticle concentration. The alpha-amylase inhibitory activity of CELFeNPs was higher than CELE for concentrations ranging from 20 to 100µg/ml. Green synthesized CELFeNPs demonstrated superior antioxidant, antibacterial, and anti-diabetic activity when compared with CELE. The results from the current research indicate that the Fe_2O_3 nanoparticles produced by green synthesis utilizing *C. roseus* ethanolic leaf extract have greater efficacy than the *C. roseus* ethanolic leaf extract and could be used as a therapeutic agent.

1. INTRODUCTION

Green nanodrug delivery systems utilizing plant extracts have shown great potential as green synthesis focuses on reducing energy use, eliminating toxic waste, and employing environmentally acceptable solvents such as ethanol, and ethyl acetate. Green methods for making nanoparticles have several benefits than chemical methods, including lack of complexity, cost-efficiency, and a quick methodology instead of using expensive or hazardous chemicals [1]. Currently, microorganisms [2] as well as root extracts, seeds, and fruits of numerous plants are mostly used in green synthesis. Because of their superparamagnetic qualities such as the ratio of the surface area to that of its volume, low toxicity, including straightforward fractionation methods, FeNPs have drawn a lot of attention [3]. They are particularly promising for protein immobilization in biomedical applications like heat therapy, magnetic resonance imaging, and drug delivery [4]. A variety of drugs can be delivered to every part of the body by utilizing functionalized Fe_2O_3 nanoparticles as a carrier. To produce the core-shell structure of targeted drug delivery carriers, biocompatible components work as a functionalized shell around iron oxide nanoparticles which are magnetic [5]. Iron oxide nanoparticles synthesized from oak leaves of *Quercus virginiana* have been shown to ameliorate Arsenic [6]. Silver nanoparticles by green synthesis utilizing *Piper longum* fruit extract have been shown to possess antioxidant properties [7].

Catharanthus roseus, frequently known by the name rose periwinkle, is a plant from the Apocynaceae family with perennial flowering. It has gained growing attention due to its antimicrobial, antioxidant, antidiabetic, and anticancer properties [8]. More than 130 bioactive compounds are produced by the plant, including the anticancer medications vinblastine and vincristine. Even today, traditional medicine use *C. roseus* plant extensively for the treatment of a range of illnesses [9]. Proteins and polyphenols which are components of plant materials can play the role of reducing agents, transforming metal ions into lower valence states instead of using chemical reagents.

Iron oxide nanoparticles have been shown to be a potential therapeutic agent. *Catharanthus roseus*, due to the presence of bioactive compounds have been shown to have strong medicinal properties. Studies are being conducted in plant-based green synthesis of nanoparticles [10] for therapy but not much work has been done in the area of green synthesized iron nanoparticles utilizing *C. roseus*. If so, a combination of both, by utilizing the extract of *C. roseus* to produce

*Corresponding Author
Priya Josson Akkara, Department of Life Sciences, Kristu Jayanti College, Bangalore, India. E-mail: priyajosson @ kristujayanti.com

© 2025 Priya Josson Akkara *et al.* This is an open access article distributed under the terms of the Creative Commons Attribution License -NonCommercial-ShareAlike Unported License (http://creativecommons.org/licenses/by-nc-sa/3.0/).

Fe_2O_3 nanoparticles by green synthesis method would enhance the effect of *C. roseus*, and would thus increase its potential as a therapeutic agent. *Catharanthus roseus*-mediated Fe_2O_3 nanoparticles would be able to execute drug delivery with enhanced efficacy as the bioactive compounds in the *C. roseus* extract are not lost by dissolution. With this aim, a comparative research of the efficacy of the green synthesized Fe_2O_3 nanoparticles of *C. roseus* extract of leaf (CELFeNPs) with that of *C. roseus* extract of leaf derived from the ethanolic fraction (CELE) was carried out in the present study to check *in vitro* antioxidant, antibacterial as well as anti-diabetic properties. Our study demonstrated enhanced antioxidant, antibacterial, and anti-diabetic properties with *C. roseus* Fe_2O_3 nanoparticles in comparison with *C. roseus* extract. These results could also open up strategies for diabetic wound healing therapy.

2. MATERIALS AND METHODS

2.1. Collection of Sample

Catharanthus roseus leaves were picked from the Ethno-medicinal Garden, Yelahanka Bangalore, Karnataka. The raw drug samples with Foundation for Revitalisation of Local Health Traditions (FRLHT) Acc. No. 6373 had been identified based on macroscopic studies of the sample (leaves, stem, and flower) in the Pharmacognosy Laboratory, FRLHT, Bengaluru, India, and was identified as belonging to the family of Apocynaceae with *C. roseus* (L.) G. Don as the botanical name, commonly named Periwinkle. The newly picked leaves were rinsed using distilled water. It was dried for roughly 24 hours at 50°C and made to powder which is fine [11].

2.2. Preparation of *C. roseus* Leaf Extract

30 g of grounded powder was soaked in 300 ml of ethanol for 1 day and thereafter extracted with the solvent ethanol using a soxhlet apparatus. After extraction for 15 cycles, the liquid extract was left to evaporate in a water bath [12]. The leaf extract (CELE) was preserved at 4°C for studies.

2.3. gas chromatography-mass spectrometry (GCMS) of CELE

The research utilized a fused column of silica that was suffused with Elite-5MS (95% dimethylpolysiloxane, 5% biphenyl, 250 µm df × 30 m × 0.25 mm ID), and was conducted using the Clarus 680 GC [13]. Helium served to be the carrier gas, maintaining a steady rate of flow at 1 ml in 1 minute to segregate the constituents. Throughout the process of chromatography, the temperature of the injector remained regulated at 260°C. The parameters for the mass detector were 240°C for the ion source, transmission line, and electron impact energy of 70 eV at 0.1-second intervals for the scan. The size of the fragments was between 40 and 600 Da. A component spectrum database was kept in reserve in the GC-MS NIST library (2008) and was compared with component spectra.

2.4. Green Synthesis of Fe_2O_3 Nanoparticles Utilising *C. roseus* Ethanolic Extract of Leaf

Extract from *C. roseus's* leaves was added to 0.1 M ferric chloride mixture at a 1:1 ratio after which incubation was carried out in a water bath for 20 minutes at 80°C for synthesizing FeNPs. It was continuously stirred for 8 hours and was left in the dark for 24 hours to settle [14]. The conversion of color from that of yellow into greyish-black confirmed the production of Fe_2O_3 nanoparticles [15]. The nanoparticles were purified by centrifuging the mixture three times for 5 minutes at a speed of 6,000 rpm using ethanol [16]. The sample (CELFeNPs) pellet was then taken on a watch glass and was dried at 60°C for a time period of 24 hours before being scraped and stored.

2.5. CELFeNPs and its Characterization

2.5.1. UV-Vis spectrometry of CELFeNPs

Thermo Scientific Genesys 180 was used for spectrophotometric assay and ethyl alcohol was used as blank. Analysis of freshly generated CELFeNPs was performed at ambient temperature (24°C–28°C) utilizing a cuvette made of quartz with a 1 cm optical path length. The formation of FeNPs was confirmed by scanning the CELFeNPs at an absorbance range of 200–300 nm. The color shift became apparent 5–10 minutes into the response [17].

2.5.2. Fourier transform-infrared spectroscopy (FTIR) spectroscopy of CELE and CELFeNPs

The FTIR analysis of *CELE* and CELFeNPs *s* was investigated at the Vellore Institute of Technology, Vellore. The features of functional groups resulting from the interaction of the nanomaterial with the attached biomolecules were evaluated using the FTIR spectrophotometer, Thermo Fisher Scientific, USA [18]. The powdered sample was processed and its FTIR spectra were captured with 20 scans at 2 cm^{-1} resolution, covering a broad extent of wavenumbers ranging from 500–4,000 cm^{-1} [19].

2.5.3. X-ray diffraction (XRD) analysis of CELFeNPs

The nature of crystallinity of the FeNPs produced from *C. roseus* was assessed by XRD analysis which was performed utilizing the diffractometer, Rigaku DMAX 2100 that employs CuK α radiation (γ = 0.154056 nm) which is monochromatic, at 30 mA and 40 kV. The necessary mask was selected and the sample was secured in the sample spinner stage. An XRD scan with an angle range of 10–80 degrees was selected. Increment in 2θ, integration (counting) time was selected, and scan results were used to identify peak positions.

2.6. Antioxidant Assay of CELE and CELFeNPs

2.6.1. Property of scavenging free radicals

The capacity of CELE and CELFeNPs to counteract the effect of free radicals was evaluated by utilizing the 2,2-Diphenyl-1-picrylhydrazyl (DPPH) assay of scavenging free radicals [20]. DPPH at 0.1 mM concentration was prepared in ethanol. 1.6 ml of sample was diluted to get a series of concentrations in ethanol covering a range of 10 µg/ml through 100 µg/ml and was blended with 2.4 ml of this mixture. Once the mixture of reactants was thoroughly vortexed, it was allowed to remain for a period of 30 minutes without exposing to light. The assessment of absorbance was made at 517 nm. The chosen standard was Ascorbic acid [21]. The test was conducted in three replicates. The equation below was used to convert the absorbance into a percentage representing antioxidant activity:

The percentage of free radical scavenging is equal to the difference between the Absorbance of the control and sample, multiplied by 100 and then, divided by the absorbance of the control.

2.6.2. Ferric reducing antioxidant power (FRAP)

For calculating the Fe^{2+} content of the samples and to determine their antioxidant capacity, a calibration curve was developed by incorporating the FRAP reagent into a series of Fe2+ solutions with a known range of concentrations. Standard iron (II) sulphate

heptahydrate was prepared, with concentrations ranging from 20 to 100µg/ml. Acetate buffer at a concentration of 30 mmol/l pH 3.6 and at a volume of 25 ml, 2.5 ml of TPTZ/HCL solution at a concentration of 10 mmol/l, ferric chloride at concentration 20 mmol/l at a volume of 2.5 ml and 40 mM HCl were mixed together to make the reagent, FRAP. A total of 30 µl of CELE/CELFeNPs was blended with 90 µl water along with 900 µl volume of the reagent, FRAP. It was allowed to incubate at 37°C for a duration of 10 minutes. Under the same incubation conditions, a blank was made using the same solution mixture but without CELE/ CELFeNPs or standard. The solution's absorbance was assessed at 593 nm wavelength. µM FeSO4/g of dried sample was determined as the value of FRAP [22]. A higher reducing capability was indicated by a reaction mixture with greater absorbance. A triplicate of the experiment was conducted.

2.7. Antibacterial Assay of CELE and CELFeNPs

The tested microorganisms comprised of *Staphylococcus aureus* including *Bacillus subtilis*, and also *Escherichia coli,* and *Pseudomonas fluorescens*. All the strains of bacteria were stored at 4 C on nutrient agar-containing slants. It was grown at 37°C in nutrient broth. Each bacterial strain was cultured in Müeller-Hinton broth (pH 7.4) for eighteen hours. A spectrophotometer was used to adjust the suspensions' concentration to 0.5 (optical density). The antibacterial property of CELFeNPs and CELE was assessed utilizing the method of Agar well diffusion [23]. Sterilized petri plates were filled with 20 ml each of sterile Nutrient agar. After solidification, sterile spreaders were used to inoculate 100 µl of each isolate's standardized inoculate onto nutrient agar plates. A sterile gel puncher with a diameter of 5 mm was made and used of to punch the wells over the agar plates. Then, the samples were solubilized in 1% (v/v) dimethylsulphoxide, which acted as the negative control for the solvent extract. Separate wells were filled with 100 µl of each sample. Three different concentrations comprising of 50, 100, and 150 µg/ml of CELE/ CELFeNPs were added in equal volumes in separate wells (100 µl) for 24 to 48 hours. Three replicates of the test per bacterial strain were maintained by incubating the plates at 37°C. The circular zone's inhibition diameter surrounding each well was measured subsequent to incubation and recorded in millimeters.

2.8. Alpha-Amylase Inhibition Activity of CELE and CELFeNPs

The DNS method was adopted to analyze alpha-amylase inhibition. The extract (CELE/ CELFeNPs) was combined with 200 µl of α-amylase solution with a concentration of 2 units ml^{-1} which was kept at 30°C for a period of 10 minutes. In each tube, 200µl of 1% solution of starch was introduced and left to incubate for 3 minutes and the process of reaction was halted by incorporating 200 µl of DNS. It was then heated for a duration of 10 minutes in a boiling water bath. 200µl of buffer served as blank and absorbance was taken at 540 nm [24]. The test sample was used at each concentration to create a blank response in which the enzyme was absent. Acarbose was utilized as a positive control. Analysis was done in triplicate. The percent of α-amylase inhibitory property was derived by the formula given below:

$$\text{α-amylase inhibition (\%)} = \frac{\text{Absorbance (control)} - \text{Absorbance (Sample)}}{\text{Absorbance (control)}} \times 100$$

2.9. Statistical Evaluation

Using version 17 of SPSS software (SPSS Inc., Chicago, IL), One-way ANOVA has been employed for statistical evaluation. As a post-test Tukey was utilized to further classify the means. *p*-values were considered significant at 5%.

3. RESULTS AND DISCUSSION

In the current study, *C. roseus* and iron oxide were used to efficiently synthesize CELFeNPs, with the phytochemicals in *C. roseus* serving as stabilizing and reducing agents. A color shift from yellow to greyish black demonstrated the preliminary synthesis of CELFeNPs [25]. The functional groups in phytochemicals including hydroxyl, carboxyl, and amino operate as both capping agents as well as efficient metal-reductants to coat the metal nanoparticles with a long-lasting coating in a single step, turning its color from yellowish brown to brownish black as stated in earlier studies [26] confirming the mechanism of green synthesized CELFeNPs in our study (Fig. 1).

By employing UV-visible spectrophotometer analysis, the stability of CELFeNPs iron oxide nanoparticles produced in an aqueous solution were verified and characterized. The size, shape, and chemical makeup of the generated FeNPs determine the formation of absorption bands and is caused by stimulation of surface plasmon vibration, which leads to aggregation. The wavelength range for the greatest UV-Vis absorption spectra was 200–310 nm and CELFeNPs showed a characteristic absorbance at a spectral range of 298 nm as shown in Figure 2 in confirmation with earlier studies [27].

Phytochemical contents of CELE was evaluated using GC-MS investigations depending on molecular weight, retention time, and the validation of MS libraries. Both the mass spectra of the major

Figure 1. Stages of preparation of CELE.

phytoconstituents as well as the GC-MS chromatogram of CELE was evaluated. Figure 3 displays the mass spectra of the major phytoconstituents found as well as the GC-MS chromatogram of CELE.

The outcome of GC-MS profiling of *C. roseus* leaf extract is shown in Table 1, which identified the presence of 10 major phytoconstituents and our results were in confirmation with earlier studies [28]. The major phytoconstituents present in CELE in our study were N-Ethyl-N'-Nitroguanidine; Butanoic Acid, 2-Hydroxy-, Methyl Ester; DL-Arabinose; 2-O-Methyl-D-Mannopyranosa; Scyllo-Inositol, 1-C-Methyl-; D-Epi-Inositol, 4-C-Methyl-; Nonadecanoic Acid; Phytol; Cyclopentanepropanol, 2-Methylene-; 7,11-Hexadecadienal; 3-Heptanone, 4-Methyl-; 3-Heptanone, 4-Methyl-; 3-[(5-Isobutyl-2-Methyl-Furan-3-Carbonyl)-Amino]-Benzoic Acid in confirmation in accordance with earlier studies [29].

Trans-phytol is a carotenoid derivative compound that has been earlier reported in *C. roseus* leaf extract [30]. Butanoic acid has been found to have antibacterial activity [31]. Mannopyranose and the enzymes associated with it have provided a valuable understanding of the forces at play in interactions with carbohydrates [32]. Scyllo-inositol considerably improves disease pathology and prevents cognitive deficits in TgCRND8 mice, indicating that it may be effective for Alzheimer's treatment [33]. 4-C-methyl-, nonadecanoic acid has been shown to have a role in anti-hepatic fibrosis [34]. Phytol including its metabolites which are pristanic and phytanic acids, could act as dietary elements in cancer prevention [35]. 5-Hydroxy-7-(4′-hydroxy-3′-methoxyphenyl)-1-phenyl-3-heptanone has shown as an inhibitor of pancreatic lipase, extracted from *Alpinia officinarum*, showing antihyperlipidemic activity. Modified as well as non-modified steroidal 4-methyl-3-bis(2-chloroethyl)amino benzoic acid esteric derivatives have demonstrated antileukemic as well as cytogenetic properties [36].

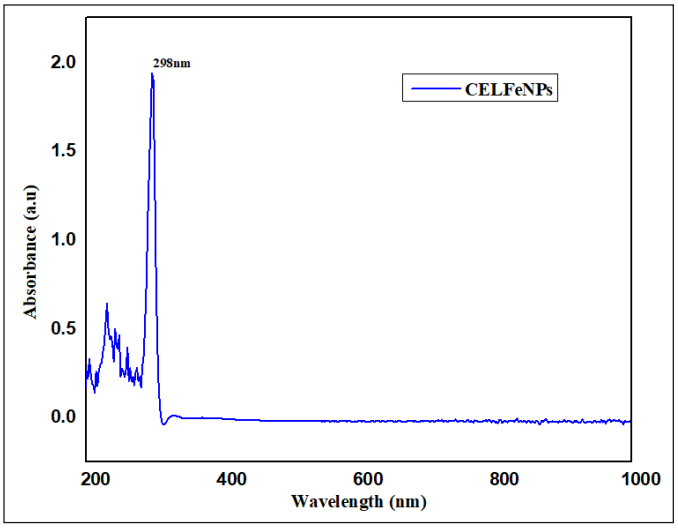

Figure 2. UV-Vis spectra of CELFeNPs.

In order to characterize and compare functional groups in CELE and CELFeNPs, FTIR was made use of by monitoring the absorption of infrared radiation (Table 2). FTIR spectra of CELE showed a variety of absorption peaks that represent their makeup as in Figure 4 the functional groups in charge of photoreducing Fe+ into FeNPs were pinpointed as in Figure 5.

The FTIR spectra of CELFeNPs showed changes in peaks of the *C. roseus* ethanolic leaf extract, with the functional groups alkene, which were absent from the FTIR spectra of FeNPs and were in charge of forming FeNPs. This peak was 1,712.88 cm^{-1}. The peak shifts following the interaction of ferric chloride with leaf extract are shown in Figure 5. Small amounts of organic acids are represented by the remaining indistinct peaks which cause the sample's low pH, which promotes FeNPs synthesis.

Alkaloids and flavonoids from the *C. roseus* extract and their functional groups not only help in the reduction process but also minimize the aggregation of nanoparticles. The stretching vibrational peaks as demonstrated by FTIR output indicate that the biomolecules act as agents for stabilization. The peak at 2,925.23 cm^{-1} that of N-H stretching of secondary/primary/amines,1,712.88 cm^{-1} that of C=C stretching correlating to alkene, 1,640.79 cm^{-1} that of amide and 947.51 cm^{-1} that of C-N stretching corresponding to amine, present in the *C. roseus* extract helps in of metal ion reduction and play the role of capping agents during iron oxide nanoparticle formation. The secondary metabolites existing in *C. roseus* extract not only contribute as fabricating agents but also enhance the stability of nanoparticles.

The sharp bands by CELFeNP at 3,288.86 cm^{-1}, 1,579.63 cm^{-1} as well as 1,384.32 cm^{-1} correlates to alcohol/phenol (O-H), aromatic groups indicating flavonoids (C=C), alkanes (C-H) stretching vibrations, while 1,261.51 cm^{-1}, 1,053.62 cm^{-1} as well as 811.58 cm^{-1} correlates to that of

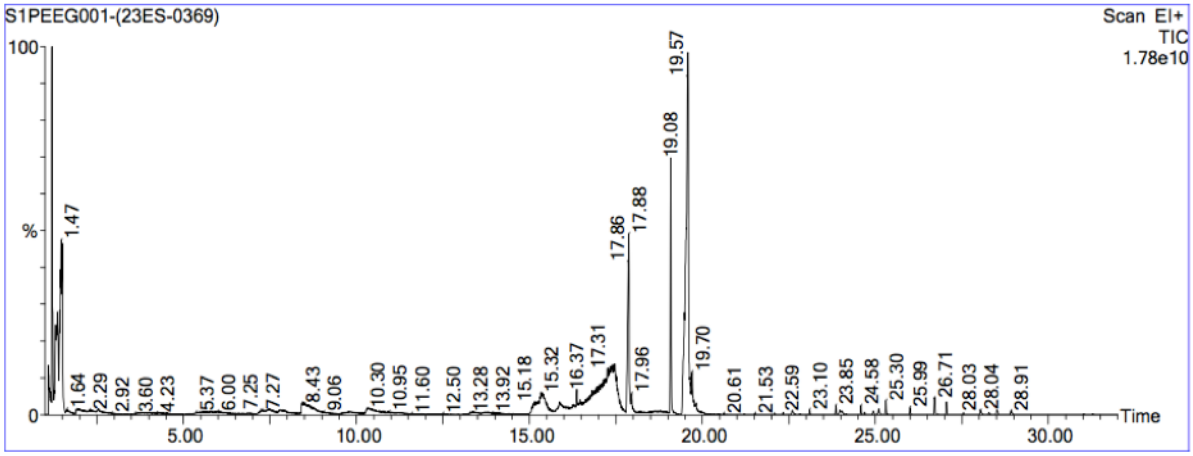

Figure 3. GC-MS profile of CELE.

Table 1. GC-MS spectrum of CELE.

Sl. No	RT	Scan	Height	Area	Area%	Norm%
1	1.474	95	7,192,686,592	294,546,720.0	8.728	20.45
2	1.504	101	7,222,917,632	190,152,320.0	5.634	13.21
3	15.374	2,874	691,838,464	116,358,560.0	3.448	8.08
4	17.135	3,226	745,590,464	65,099,536.0	1.929	4.52
5	17.255	3,250	1,442,556,032	111,715,424.0	3.310	7.76
6	17.465	3,292	1,906,566,528	417,210,944.0	12.363	28.97
7	17.875	3,374	8,374,007,004	304,580,576.0	11.602	27.40
8	19.081	3,615	12,330,670,080	295,315,456.0	8.751	20.51
9	19.586	3,716	16,840,475,648	1,439,980,288.0	42.669	100.00
10	19.701	3,739	1,474,153,472	49,843,412.0	1.477	3.46

Table 2. FTIR absorbance peak values and correlation to functional groups in CELE and CELFeNPs.

Compounds	Sl. No.	Peak value (cm^{-1})	Peak assignments	Functional groups
CELE	1	3,358.98	O-H stretch	Alcohol, Phenol
	2	2,925.23	N-H stretch	1˚ or 2˚ Amine
	3	1,,712.88	C=C bending	Alkene
	4	1377.06	C-H bending	Alkane
	5	1,049.64	C-O stretch	1˚ or 2˚ alcohol
	6	947.51	C-N stretch	Amine
	7	815.94	C-Cl stretch	Chloroalkanes
CELFeNPs	1	3,288.86	O-H stretch	Alcohol, Phenol
	2	2,936.59	N-H stretch	1˚ or 2˚ Amine
	3	1,579.63	C=C bending	Aromatic
	4	1,384.32	C-H bending	Alkane
	5	1,261.51	C-N stretch	Amine
	6	1,053.62	C-O stretch	1˚ or 2˚ alcohol
	7	811.58	C-Cl stretch	Chloroalkanes

aliphatic amine groups of alkaloids (C=N), primary/secondary alcohol (C-O) and chloroalkene (C-Cl). Peaks at 3,292.84, 2,927.78, 1,638.55, 1,350.99, and 1,026.60 cm^{-1} were observed in iron nanoparticles that were made from Citrus maxima peel which is in correlation with the peaks by CELFeNPs in our study [37]. Alkenes, Phosphate, hydroxyl, and carboxyl acid groups were found in green synthesized iron oxide nanoparticles employing *Anastatica hierochuntica* in confirmation with our FTIR spectra for CELFeNPs [38].

The phases and the characteristics of the nanoparticles were mainly determined by the peaks observed in the pattern of XRD, as demonstrated in Figure 6. The width of the peak indicated the typical crystalline size of the nanoparticle; broader peaks signified minute crystallites, whereas narrower peaks indicated bigger crystallites. The sample's imperfections would be caused by the crystal structure flaws, microstains, component heterogeneity, and size of the crystallite.

The XRD analysis of the Fe_2O_3 nanoparticles which were synthesized demonstrated peaks at 2Θ positioned 33.54˚, 41.40˚, 45.10˚, 53.54˚, 57.26˚, and 68.70˚and the observed lattice spacings at are well matched with that of (220), (311), (400), (511), (422), and (440) planes of Fe_2O_3 crystals. The data on the crystal structure closely

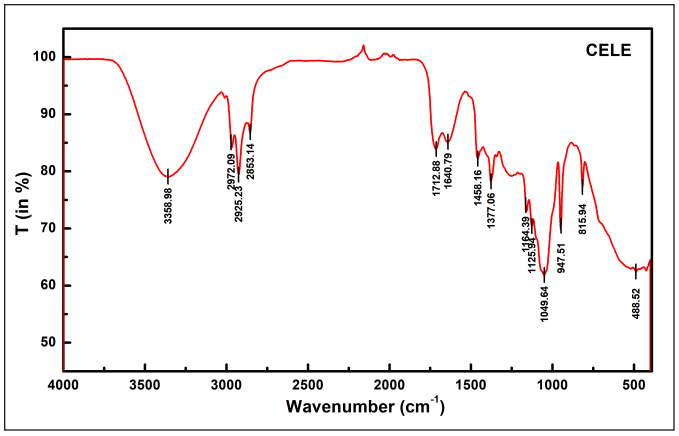

Figure 4. FTIR spectra of CELE.

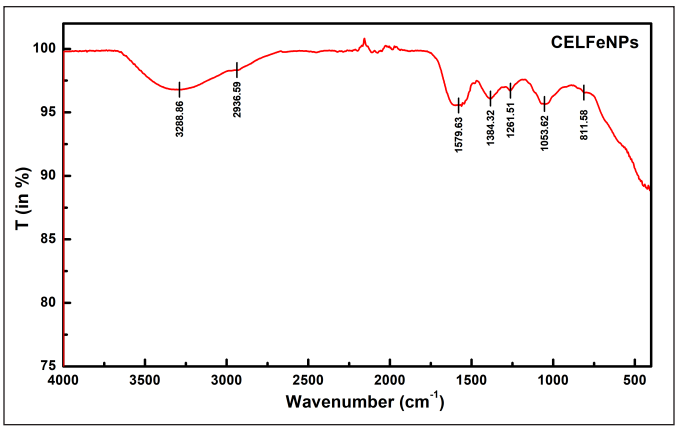

Figure 5. FTIR spectra of CELFeNPs.

aligns with the reported information, confirming its assignment to the iron oxide magnetite phase [39]. The pattern of XRD obtained for the nanoparticles is compared with the International Centre for Diffraction Data file No.: 00–019-0629. The synthesized FeNPs exhibited peak intensities varying from 240 to 1,400 arbitrary units. These outcomes closely align with findings from previous studies on iron oxide nanoparticles and it has been observed that temperature has a role in the crystalline nature of Fe_2O_3 nanoparticles which were synthesized in a sustainable way [40]. The distinct and well-defined peaks show the nature of crystalline Fe_2O_3 nanoparticles synthesized through the reduction method utilizing *C. roseus* leaf extract in our work.

Calculation of the average of crystalline crystal size (D) is executed by utilizing the Debye-Scherrer formula.

$$D = \frac{K\,\lambda}{\beta\,\cos\,\theta}$$

wherein K represents a constant value of 0.89, λ denotes the X-rays wavelength (1.5406 Å), β indicates the half maximum full width whereas θ refrs to the angle at which diffraction occurs at half the maximum. The dislocation density (δ) is assessed utilizing the formula δ = n/D2, wherein n equals 1, signifying the order of diffraction. The average size of the crystallite size was 0.71625 nm (Table 3).

CELFeNPs had the highest Fe3+ reduction in the FRAP assay demonstrating the enhancement of antioxidant activity in green synthesized nanoparticles (Fig. 7a) which correlates with the

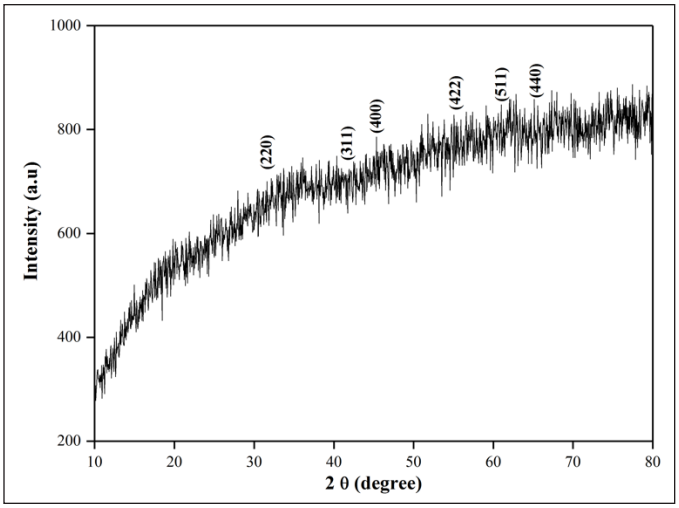

Figure 6. XRD pattern of synthesized CELFeNPs.

Table 3. XRD parameters for calculation of crystallite size.

2θ	d-spacing (Å)	FWHM	Crystallite size D (nm)	δ (10^{-2} nm^{-2})
18.854	4.703	0.4132	0.332	9.082
18.001	4.924	0.3691	0.407	6.018
60.028	1.539	0.4603	1.772	0.318
74.713	1.269	0.4106	0.354	7.956

results of antioxidant activity of graphene/chitosan functionalized superparamagnetic *C. roseus* Fe_2O_3 nanoparticles [41]. The results of free radical scavenging activity by DPPH demonstrated that in comparison to the standard, the percentage of antioxidant activity of *C. roseus* (CELE) was 69.88%, while the green synthesized nanoparticles (CELFeNPs) showed better antioxidant activity at 76% as in Figure 7b. The antioxidant activity of CELFeNPs could be utilized for targeting disorders related to elevated oxidative stress. Cerium oxide-containing nanoparticles have been shown to efficiently scavenge radicals, reducing oxidative stress in model cell lines. The reducing power of CELE demonstrated its strong antioxidant potential due to secondary metabolites in *C. roseus*, which may contribute to a reduction in oxidative stress as confirmed by earlier studies [42].

The well diffusion procedure was utilized to analyze the antibacterial effects of CELE and CELFeNPs [43]. The zones of inhibition of CELFeNPs and CELE against *P. fluorescence, S. aureus, B. subtilis*, and *E. coli* were analyzed. It was shown that *C. roseus*-iron oxide nanoparticles showed concentration-dependent antibacterial activity, demonstrating that the extract's antibacterial potency grows with its concentration against the test organism (Table 4).

The results shown in Table 3 concludes that CELFeNPs have the highest antimicrobial activity against the test organisms compared to CELE. The zone of inhibition was maximum with CELFeNPs against *S. aureus*. The last activity was witnessed with the CELFeNPs against *B. subtilis* indicating that CELFeNPs are not effective against *B. subtilis*. CELFeNPs demonstrated anti-bacterial properties against *S. aureus, E. coli,* and *P. fluorescence* (Fig. 9). As per the findings, Gram-negative bacteria are found to be more effectively combatted than gram-positive bacteria. Iron oxide nanoparticles with *Tridax procumbens*

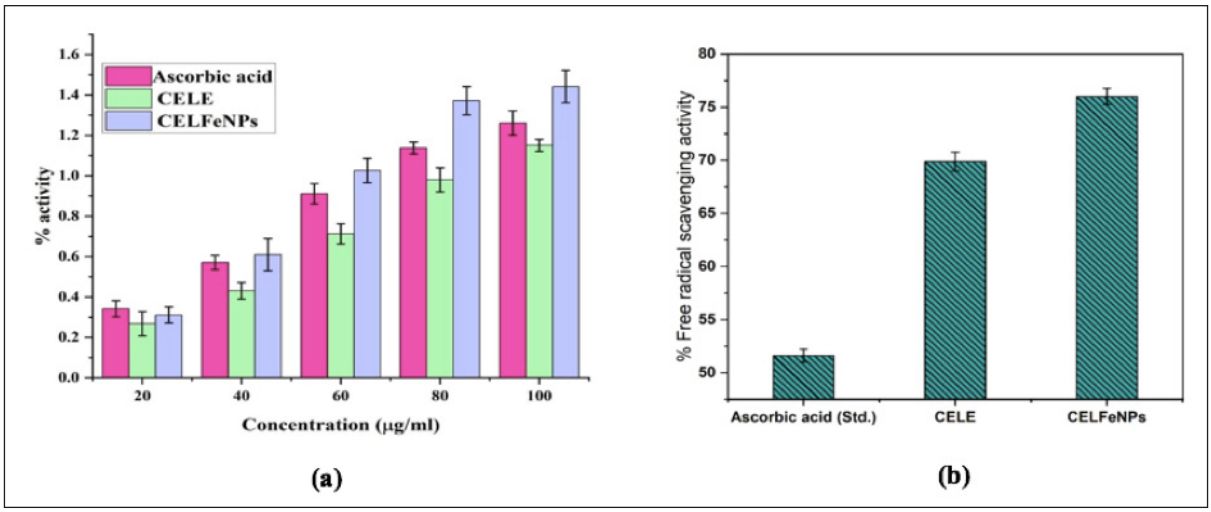

Figure 7. Anti-oxidant activity: scavenging activity of percentage of ascorbic acid (std.), CELE and CELFeNPs (a) FRAP assay; (b) DPPH assay.

Table 4. Antibacterial activity of CELE and CELFeNPs.

Sl. No	Organism	Zone of inhibition (mm)							
		CELE (µg/ml)				CELFeNPs (µg/ml)			
		50	100	150	control	50	100	150	control
1	*Escherichia coli*	No Zone	No Zone	4.0 ± 0.2	5.0 ± 0.1	No Zone	8.5 ± 0.2	10.0 ± 0.1	17.2 ± 0.1
2	*Staphylococcus aureus*	3.0 ± 0.2	5.0 ± 0.2	5.2 ± 0.1	5.5 ± 0.1	10.2 ± 0.1	11.0 ± 0.1	15.2 ± 0.1	18.5 ± 0.1
3	*Bacillus subtilis*	No Zone	No Zone	2.0 ± 0.2	2.0 ± 0.2	No Zone	No Zone	8.0 ± 0.1	No Zone
4	*Pseudomonas fluorescence*	No Zone	No Zone	7.0 ± 0.1	7.0 ± 0.2	10.4 ± 0.1	10.4 ± 0.1	12.3 ± 0.1	19.2 ± 0.2

and CELFeNPs has been shown to have an antibacterial effect against gram-negative bacteria, similar to our reports [44,45]. Curcumin-loaded dextran-coated iron oxide nanoparticles have demonstrated antimicrobial properties [46].

The presence of butanoic acid in our GCMS analysis of CELE might be a contributing factor to the anti-bacterial effect of CELFeNPs as the effectiveness of butanoic acid in combating pathogens to bacteria including *Staphylococcus pseudintermedius* and *Acinetobacter baumannii* has been reported [31]. Recent research have demonstrated that nanoparticles with Iron have been found to promote healing in chronic wounds pertaining to bacterial infection [47]. *Catharanthus roseus* leaf extract has been shown to have wound-healing activity [48]. Our results emphasize the efficacy of CELFeNPs over CELE. This could be metal ion release from CELFeNPs which aids in wound healing by its antibacterial activity.

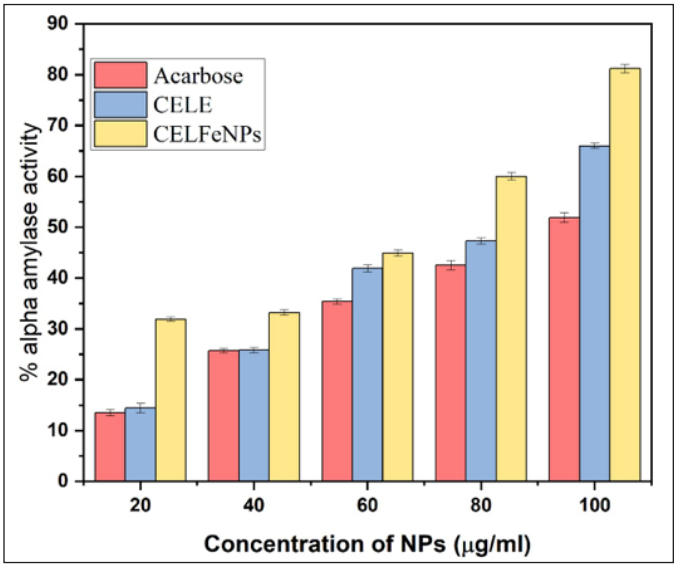

Figure 8. Alpha amylase inhibitory activity of Acarbose (Std), CELE and CELFeNPs.

Catharanthus roseus leaf extract has been shown to possess an anti-diabetic effect by blocking important enzymes in the process of breaking down carbohydrates, such as alpha-amylase [49]. In our study, the CELE and CELFeNPs showed significant inhibitory activity of alpha-amylase in comparison with Acarbose, used as standard. It was observed that the alpha-amylase inhibition of CELFeNPs was greater than that of CELE with significance at concentrations ranging from 20 to 100 µg/ml with a maximum at 100 µg/ml emphasizing the fact that CELFeNPs might have a better antidiabetic activity compared with *C. roseus* extract (Fig. 8). Our reports are in correlation with the results of Shabbir *et al*. [50] that Fe_2O_3 nanoparticles from plant extract of *Madhuca indica* showed inhibition of α-amylase, which was more than that of the control used, confirming the antidiabetic activity.

Catharanthus roseus ethanolic extract (CELE) of leaves was utilized as a reducing, and also green capping agent in an environmentally friendly method of synthesis to create Fe_2O_3 nanoparticles in our study [39]. The bioactive components of CELE were evaluated by GC-MS which demonstrated the presence of ten significant phytoconstituents. UV-Vis spectra confirmed the NPs formation by demonstrating the peak at the wavelength of 298 nm. The *C. roseus*

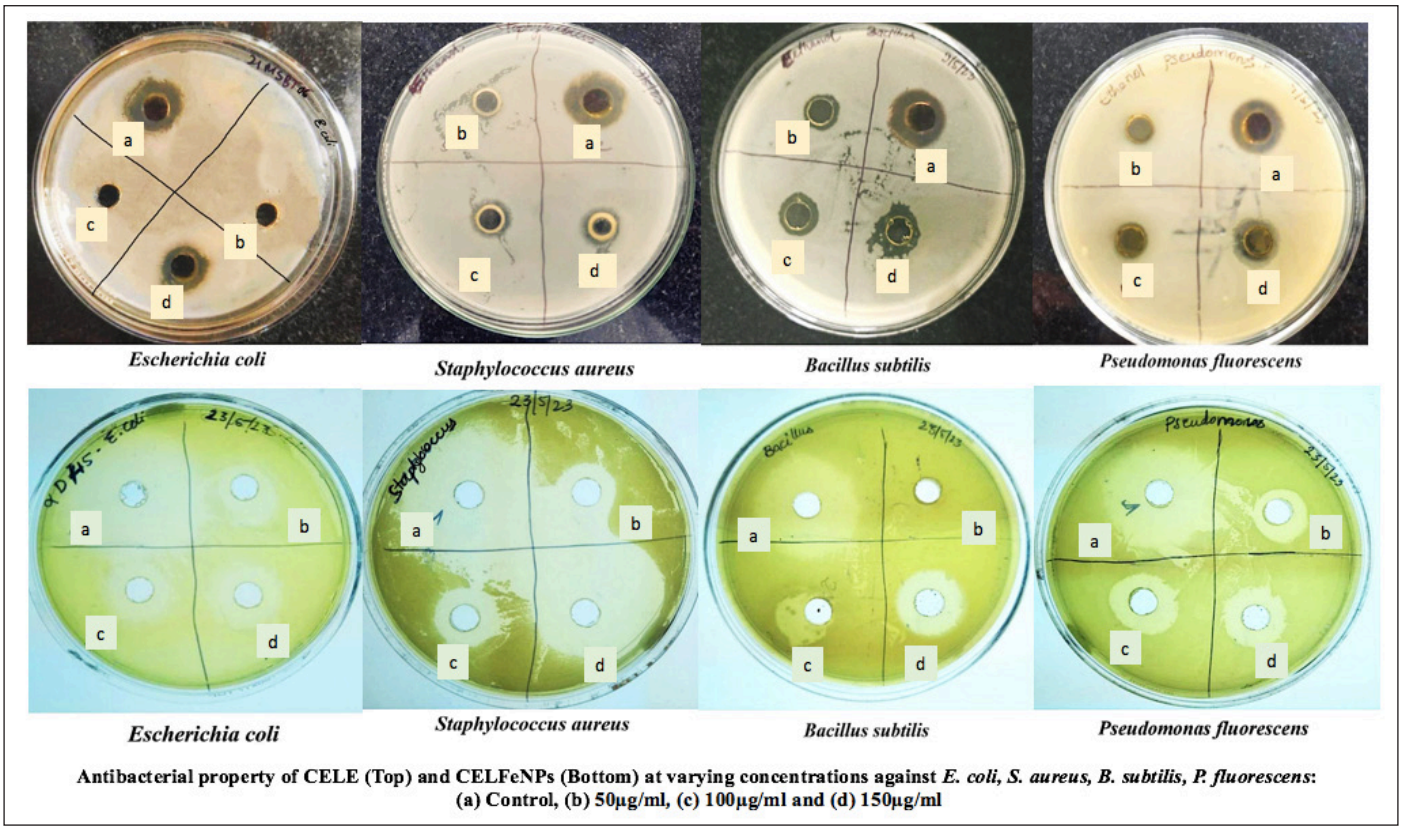

Figure 9. Zones of inhibition of CELE and CELFeNPs.

plant extract stabilizes the nanoparticles and acts as a reducing agent [51]. The effective stabilization and capping capabilities of FeNPs were demonstrated by FTIR analysis. The phase identity and crystalline nature were validated by XRD analysis. Our results show that *C. roseus* has a strong antioxidant potential because it contains several secondary metabolites in the crude extract, including proteins, flavonoids, alkaloids, and phenols [52]. Additionally, the results showed that secondary metabolites in leaf extract have substantial antibacterial and alpha-amylase inhibition activity [53]. The potential compounds which are bioactive present in the *C. roseus* might contribute to antidiabetic properties [54] as shown in our results.

4. CONCLUSION

According to the results of the inquiry, the CELFeNPs synthesized by the eco-friendly method have better antioxidant, antimicrobial, and alpha-amylase inhibition property, in comparison with that of the CELE of leaves. As the results show antimicrobial and alpha-amylase inhibition, it could also be effective as an agent for diabetic wound healing. Further studies can be done to comprehend the mechanistic action of green synthesized CELFeNPs as a therapeutic agent.

5. AUTHORS' CONTRIBUTION

All authors made substantial contributions to conception and design, acquisition of data, or analysis and interpretation of data; took part in drafting the article or revising it critically for important intellectual content; agreed to submit to the current journal; gave final approval of the version to be published; and agree to be accountable for all aspects of the work. All the authors are eligible to be an author as per the International Committee of Medical Journal Editors (ICMJE) requirements/guidelines.

6. ACKNOWLEDGMENTS

We acknowledge the SIF Lab of VIT, Chemistry Division of SAS for FTIR, GC-MS, and XRD Analysis.

7. FUNDING

There is no funding to report.

8. CONFLICTS OF INTEREST

The authors report no financial or any other conflicts of interest in this work.

9. ETHICAL APPROVALS

This study does not involve experiments on animals or human subjects.

10. DATA AVAILABILITY

All the data is available with the authors and shall be provided upon request.

11. PUBLISHER'S NOTE

All claims expressed in this article are solely those of the authors and do not necessarily represent those of the publisher, the editors and the reviewers. This journal remains neutral with regard to jurisdictional claims in published institutional affiliation.

12. USE OF ARTIFICIAL INTELLIGENCE (AI)-ASSISTED TECHNOLOGY

The authors declares that they have not used artificial intelligence (AI)-tools for writing and editing of the manuscript, and no images were manipulated using AI.

REFERENCES

1. Vetrimani A, Geetha K, Jemima EA, Arulnathan N, Kim HS, Kathalingam A. Effect of the green synthesis of CuO plate-like nanoparticles on their photodegradation and antibacterial activities. Phys Chem Chem Phys 2022;24(47):28923–33; doi: http://dx.doi.org/10.1039/D2CP03531F
2. Arsiya F, Sayadi MH, Sobhani S. Green synthesis of palladium nanoparticles using *Chlorella vulgaris.* Mater Lett 2016;186:113–5; doi: https://doi.org/10.1016/j.matlet.2016.09.101
3. Kumar A, Singhal A. Synthesis of colloidal β-Fe2O3 nanostructures-influence of addition of Co2+ on their morphology and magnetic behavior. J Nanotech 2007;18:475703; doi: https://doi.org/10.1088/0957-4484/18/47/475703
4. Hasany SF, Ahmed I, Rajan J, Rehman A. Systematic review of the preparation techniques of iron oxide magnetic nanoparticles. J Nanosci Nanotechnol 2013;2(6):148–58; doi: https://doi.org/10.5923/j.nn.20120206.01
5. Laurent S, Forge D, Port M, Roch A, Robic C, Elst LV, *et al.* Magnetic iron oxide nanoparticles: synthesis, stabilization, vectorization, physicochemical characterizations, and biological applications. Chem Rev 2010;110:2574; doi: https://doi.org/10.1021/cr068445e
6. Kamath V, Chandra P, Jeppu GP. Comparative study of using five different leaf extracts in the green synthesis of iron oxide nanoparticles for removal of arsenic from water. Int J Phytoremediation 2020;22(12):1278–94; doi: https://doi.org/10.1080/15226514.2020.1765139
7. Reddy NJ, Vali DN, Rani M, Rani SS. Evaluation of antioxidant, antibacterial and cytotoxic effects of green synthesized silver nanoparticles by *Piper longum* fruit. Mater Sci Eng C Mater Biol Appl 2014;34:115–22; doi: https://doi.org/10.1016/j.msec.2013.08.039
8. Pham HNT, Sakoff JA, Vuong QV, Bowyer MC, Scarlett CJ. Screening phytochemical content, antioxidant, antimicrobial and cytotoxic activities of *Catharanthus roseus* (L.) G. Don stem extract and its fractions. Biocatal Agric Biotechnol 2018;16:405–11; doi: https://doi.org/10.1016/j.bcab.2018.09.005
9. Nejat N, Valdiani A, Cahill D, Tan YH, Maziah M, Abiri R. Ornamental exterior versus therapeutic interior of Madagascar periwinkle (*Catharanthus roseus*): the two faces of a versatile herb. *Sci World J 2015;2015:*982412; doi: https://doi.org/10.1155/2015/982412
10. Hano C, Abbasi BH. Plant-based green synthesis of nanoparticles: production, characterization and applications. Biomolecules 2021;12(1):31; doi: https://doi.org/10.3390/biom12010031
11. Kabesh K, Senthilkumar P, Ragunathan R, Kumar RR. Phytochemical analysis of *Catharanthus roseus* plant extract and its antimicrobial activity. Int J Pure App Biosci 2015;3(2):162–72.
12. Pham HNT, Sakoff JA, Vuong QV, Bowyer MC, Scarlett CJ. Phytochemicals derived from *Catharanthus roseus* and their health benefits. Technologies 2020;8(4):80; doi: https://doi.org/10.3390/technologies8040080
13. Gomathi D, Kalaiselvi M, Ravikumar G, Devaki K, Uma C. GC-MS analysis of bioactive compounds from the whole plant ethanolic extract of *Evolvulusalsinoides* (L.) L. J Food Sci Technol 2015;52(2):1212–7; doi: https://doi.org/10.1007/s13197-013-1105-9

14. Nahari MH, Al Ali A, Asiri A, Mahnashi MH, Shaikh IA, Shettar AK. Green synthesis and characterization of iron nanoparticles synthesized from aqueous leaf extract of *Vitex leucoxylon* and its biomedical applications. Nanomaterials (Basel, Switzerland.) 2022;12(14):2404; doi: https://doi.org/10.3390/nano12142404
15. Ali A, Zafar H, Zia M, Haq IU, Phull AR, Ali JS, *et al.* Synthesis, characterization, applications, and challenges of iron oxide nanoparticles. Nanotechnol Sci Appl 2016;9:49–67; doi: https://doi.org/10.2147/NSA.S99986
16. Benzie IF, Strain JJ. The ferric reducing ability of plasma (FRAP) as a measure of "antioxidant power": the FRAP assay. Anal Biochem 1996;239(1):70–6; doi: https://doi.org/10.1006/abio.1996.0292
17. Felt DR, Larson SL, Valente EJ. UV-VIS spectroscopy of 2,4,6-trinitrotoluene-hydroxide reaction. Chemosphere 2002;49(3):287–95; doi: https://doi.org/10.1016/s0045-6535(02)00283-7
18. Krysa M, Szymańska-Chargot M, Zdunek A. FT-IR and FT-Raman fingerprints of flavonoids—a review. Food Chem 2022;393:133430; doi: https://doi.org/10.1016/j.foodchem.2022.133430
19. Rahuman HBH, Dhandapani R, Narayanan S, Palanivel V, Paramasivam R, Subbarayalu R, *et al.* Medicinal plants mediated the green synthesis of silver nanoparticles and their biomedical applications. IET Nanobiotechnol 2022;16(4):115–44; doi: https://doi.org/10.1049/nbt2.12078
20. Desmarchelier C, Bermudez MJN, Coussio J, Ciccia G, Boveris A. Antioxidant and prooxidant activities in aqueous extract of Argentine plants. Int J Pharmacogn 1997;35(2):116–20; doi: http://dx.doi.org/10.1076/phbi.35.2.116.13282
21. Munteanu IG, Apetrei C. Analytical methods used in determining antioxidant activity: a review. Int J Mol Sci 2021;22(7):3380; doi: https://doi.org/10.3390/ijms22073380
22. Dash A, Ahmed MT, Selvaraj R. Mesoporous magnetite nanoparticles synthesis using the *Peltophorum pterocarpum* pod extract, their antibacterial efficacy against pathogens and ability to remove a pollutant dye. J Mol Struct 2019;1178:268–73; doi: https://doi.org/10.1016/j.molstruc.2018.10.042
23. Arora DS, Kaur J. Antimicrobial activity of spices. Int J Antimicrob Agents 1999;12(3):257–62; doi: https://doi.org/10.1016/s0924-8579(99)00074-6
24. Wickramaratne MN, Punchihewa JC, Wickramaratne DB. *In-vitro* alpha amylase inhibitory activity of the leaf extracts of *Adenanthera pavonina*. BMC Compl Alt Med 2016;16(1):466; doi: https://doi.org/10.1186/s12906-016-1452-y
25. Lesiak B, Rangam N, Jiricek P, Gordeev I, Tóth J, Kövér L, *et al.* Surface study of Fe3O4 nanoparticles functionalized with biocompatible adsorbed molecules. Front Chem 2019;7:642; doi: https://doi.org/10.3389/fchem.2019.00642
26. Sajid M, Płotka-Wasylka J. Nanoparticles: synthesis, characteristics, and applications in analytical and other sciences. Microchem J 2020;154:104623; doi: http://dx.doi.org/10.1016/j.microc.2020.104623
27. Jeevanandam J, Ling JKU, Barhoum A, Chan YS, Danquah MK. Bionanomaterials: definitions, sources, types, properties, toxicity, and regulations. Fund Bionanomat 2022;4(5):1–29; doi: https://doi.org/10.1016/B978-0-12-824147-9.00001-7
28. Kanthal LK, Dey A, Satyavathi K, Bhojaraju P. GC-MS analysis of bio-active compounds in methanolic extract of *Lactucaruncinata* DC. Pharmacogn Res 2014;6(1):58–61; doi: https://doi.org/10.4103/0974-8490.122919
29. Olivia NU, Goodness UC, Obinna OM. Phytochemical profiling and GC-MS analysis of aqueous methanol fraction of *Hibiscus asper* leaves. Futur J Pharm Sci 2021;7:59; doi: https://doi.org/10.1186/s43094-021-00208-4
30. De Pinho PG, Gonçalves RF, Valentão P, Pereira DM, Seabra RM, Andrade PB, *et al.* Volatile composition of *Catharanthus roseus* (L.) G. Don using solid-phase microextraction and gas chromatography/mass spectrometry. J Pharm Biomed Anal 2009;49(3):674–85; doi: https://doi.org/10.1016/j.jpba.2008.12.032
31. Kennedy GM, Min MY, Fitzgerald JF, Nguyen MT, Schultz SL, Crum MT, *et al.* Inactivation of the bacterial pathogens *Staphylococcus pseudintermedius* and *Acinetobacter baumannii* by butanoic acid. J Appl Microbiol 2019;126(3):752–63; doi: https://doi.org/10.1111/jam.14180
32. Moothoo DN, Canan B, Field RA, Naismith JH. Man alpha1-2 Man alpha-OMe-concanavalin A complex reveals a balance of forces involved in carbohydrate recognition. Glycobiology 1999;9(6):539–45; doi: https://doi.org/10.1093/glycob/9.6.539
33. Fenili D, Brown M, Rappaport R, McLaurin J. Properties of scyllo-inositol as a therapeutic treatment of AD-like pathology. J Mol Med (Berl) 2007;85(6):603–11; doi: https://doi.org/10.1007/s00109-007-0156-7
34. Fu W, Zhao Y, Xie J, Yang Y, Xiao P. Identification of anti-hepatic fibrosis components in *Periplaneta americana* based on spectrum-effect relationship and chemical component separation. Biomed Chromatogr 2022;36(3):e5286; doi: https://doi.org/10.1002/bmc.5286
35. Bhati M. Biogenic synthesis of metallic nanoparticles: principles and applications. Mater Today Proc 2023;81:882–7; doi: https://doi.org/10.1016/j.matpr.2021.04.272
36. Fousteris MA, Koutsourea AI, Arsenou ES, Papageorgiou A, Mourelato D, Nikolaropoulos SS. Antileukemic and cytogenetic effects of modified and non-modified esteric steroidal derivatives of 4-methyl-3-bis(2-chloroethyl)amino benzoic acid (4-Me-CABA). Anticancer Res 2002;22(4):2293–9.
37. Wei Y, Fang Z, Zheng L, Tan L, Tsang EP. Green synthesis of Fe nanoparticles using *Citrus maxima* peels aqueous extracts. Mater Lett 2016;185:384–6; doi: http://dx.doi.org/10.1016/j.matlet.2016.09.029
38. Vahini M, Rakesh SS, Subashini R, Loganathan S, Prakash DG. *In vitro* biological assessment of green synthesized iron oxide nanoparticles using *Anastatica hierochuntica* (Rose of Jericho). Biomass Conv Bioref 2023;14(16):1–11; doi: http://dx.doi.org/10.1007/s13399-023-04018-x
39. Kiwumulo HF, Muwonge H, Ibingira C, Lubwama M, Kirabira JB, Ssekitoleko RT. Green synthesis and characterization of iron-oxide nanoparticles *using Moringa oleifera*: a potential protocol for use in low and middle income countries. BMC Res Notes 2022;15(1):1–8; doi: https://doi.org/10.1186/s13104-022-06039-7
40. Ahmmad B, Leonard K, Islam MS, Kurawaki J, Muruganandham M, Ohkubo T, *et al.* Green synthesis of mesoporous hematite (α-Fe_2O_3) nanoparticles and their photocatalytic activity. Adv Powder Technol 2013;24(1):160–67; doi: https://doi.org/10.1016/j.apt.2012.04.005
41. Hastak V, Bandi S, Kashyap S, Singh S, Luqman S, Lodhe M, *et al.* Antioxidant efficacy of chitosan/graphene functionalized superparamagnetic iron oxide nanoparticles. J Mater Sci Mater Med 2018;29(10):154; doi: https://doi.org/10.1007/s10856-018-6163-0
42. Nisar A, Mamat AS, Hatim MI, Aslam MS, Ahmad MS. Antioxidant and total phenolic content of *Catharanthus roseus* using deep eutectic solvent. Rec Adv Biol Med 2017;03:1283; doi: http://dx.doi.org/10.18639/RABM.2017.03.355635
43. Gupta M, Tomar RS, Kaushik S, Mishra RK, Sharma D. Effective antimicrobial activity of green ZnO nanoparticles of *Catharanthus roseus*. Front Microbiol 2018;9:2030; doi: https://doi.org/10.3389/fmicb.2018.02030
44. Senthil M, Ramesh C. Biogenic synthesis of Fe_3O_4 nanoparticles using *Tridax procumbens* leaf extract and its antibacterial activity on *Pseudomonas aeruginosa*. Dig J Nanomater Biostructures 2012;7(4):1655–60.
45. Senthilkumar S, Siva E, Rajendran A. Characterization and antimicrobial activity of ECO-friendly biosynthesis of silver nanoparticles using an aqueous leaf extract of *Catharanthus roseus*. IOSR J App Phys 2017;01(01):71–5.

46. Bobe G, Zhang Z, Kopp R, Garzotto M, Shannon J, Takata Y. Phytol and its metabolites phytanic and pristanic acids for risk of cancer: current evidence and future directions. Eur J Cancer Prev 2020;29(2):191–200; doi: https://doi.org/10.1097/CEJ.0000000000000534
47. Lu Z, Yu D, Nie F, Wang Y, Chong Y. Iron nanoparticles open up new directions for promoting healing in chronic wounds in the context of bacterial infection. Pharmaceutics 2023;15(9):2327; doi: https://doi.org/10.3390/pharmaceutics15092327
48. Akkara PJ, Martin SA, Tomy AM, Menon AS, Takri G. Methanolic leaf extract of *Catharanthus roseus* reveals wound healing activity on mouse fibroblast L92 cell lines. Med Plants Int J Phytomed 2023;15(03):587–94.
49. Rasineni K, Bellamkonda R, Singareddy SR, Desireddy S. Antihyperglycemic activity of *Catharanthus roseus* leaf powder in streptozotocin-induced diabetic rats. Pharmacogn Res 2010;2(3):195–201; doi: https://doi.org/10.4103/0974-8490.65523
50. Shabbir MA, Naveed M, ur Rehman S, ul Ain N, Aziz T, Alharbi M, et al. Synthesis of iron oxide nanoparticles from Madhuca indica plant extract and assessment of their cytotoxic, antioxidant, anti-inflammatory, and anti-diabetic properties via different nanoinformatics approaches. ACS Omega 2023;8(37):33358–66; doi: https://doi.org/10.1021/acsomega.3c02744
51. Yadwade R, Kirtiwar S, Ankamwar B. A review on green synthesis and applications of iron oxide nanoparticles. J Nanosci Nanotechnol 2021;21(12):5812–34; doi: https://doi.org/10.1166/jnn.2021.19285
52. Goboza M, Meyer M, Aboua YG, Oguntibeju OO. *In vitro* antidiabetic and antioxidant effects of different extracts of *Catharanthus roseus* and its indole alkaloid, vindoline. Molecules 2020;25(23):5546; doi: https://doi.org/10.3390/molecules25235546
53. Kumar S, Narwal S, Kumar V, Prakash O. α-Glucosidase inhibitors from plants: a natural approach to treat diabetes. Pharmacogn Rev 2011;5(9):9; doi: https://doi.org/10.4103/0973-7847.79096
54. Khadayat K, Marasini BP, Gautam H, Ghaju S, Parajuli N. Evaluation of the alpha-amylase inhibitory activity of Nepalese medicinal plants used in the treatment of diabetes mellitus. Clin Phytosci 2020;6:34; doi: https://doi.org/10.1186/s40816-020-00179-8

How to cite this article:
Akkara PJ, Martin SA, Thiagarajulu N, Bisht AB, Mishal A, Mathew CM. Green synthesised *Catharanthus roseus* -mediated iron oxide nanoparticles demonstrates enhanced antibacterial, antioxidant, and anti-diabetic properties. J Appl Biol Biotech. 2025;13(4):126-135. DOI: 10.7324/JABB.2025.220729.